Effects of Anthracene and Pyrene Units on the Interactions of Novel Polypyridylruthenium(II) Mixed-Ligand Complexes with DNA

Mariappan Mariappan*[a] and Bhaskar G. Maiya[a][†]

Keywords: DNA cleavage / Electrophoresis / Inhibitors / N ligands / Radicals / Ruthenium

2-(9-Anthryl)-1*H*-imidazo[4,5-*f*][1,10]phenanthroline (aip) and [2-(1-pyrenyl)-1*H*-imidazo[4,5-*f*][1,10]phenanthroline (pyip) and their complexes $[Ru(phen)_2(aip)]^{2+}$ (**1**) and $[Ru(phen)_2(pyip)]^{2+}$ (**2**) (phen = 1,10-phenanthroline) have been synthesized and characterized by elemental analysis, UV/Vis, IR and ^1H NMR spectroscopy, FAB-MS and cyclic voltammetry methods. Both **1** and **2** are redox-active and undergo oxidation at 1.43 and 1.47 V (vs. SCE), respectively. Both **1** and **2** show only the ^{3}MLCT emission typical of any polypyridylruthenium(II) complex. These new complexes are seen to be excellent binders of calf-thymus (CT) DNA, as revealed by the results of absorption, luminescence, viscometric titrations, and thermal denaturation studies. These results also indicate that while ruthenium-bound aip and pyip intercalate within the base pairs of the duplex, the phen moieties act only as spectator ligands in each case. Steady-state emission studies carried out in aqueous media with and without DNA reveal that $[Ru(phen)_2(pyip)]^{2+}$ is a better "molecular light switch" for DNA than $[Ru(phen)_2(aip)]^{2+}$. Under an identical set of experimental conditions of light and drug dose, the DNA photocleavage ability of $[Ru(phen)_2(pyip)]^{2+}$ is also higher than that of $[Ru(phen)_2(aip)]^{2+}$. "Inhibitor studies" suggest that the oxygen species are mainly responsible for the DNA photocleavage by these complexes.

Introduction

Considerable attention is being directed towards the design of DNA-binding and -photocleaving ruthenium(II) complexes in order to develop novel therapeutic agents, chemical probes for nucleic acids, and novel diagnostic agents targeted to double-helical DNA.[1–4] Presently, most attention has centered upon metal complexes that are capable of binding DNA by intercalation.[5–11] Due to their luminescent characteristics and strong DNA-binding affinity, the polypyridylruthenium(II) class of metallointercalators have received particular attention.[12–14] Barton and co-workers have shown that the strong binding of $[Ru(L)_2(dppz)]^{2+}$ complexes (L = 2,2′-bipyridine or 1,10-phenanthroline) to DNA gives rise to the "molecular light-switch effect", where the nearly undetectable emission from the triplet metal-to-ligand charge transfer (MLCT) excited state of $[Ru(L)_2(dppz)]^{2+}$ in water is strongly enhanced due to the intercalation of the planar dppz ligand between the base pairs of DNA.[10,15–17] One important characteristic of these ligands is that they all possess extended π-aromatic structures and are planar, which is crucial for the intercalation of the Ru^{II} complexes containing them. In our efforts to design metal complexes coordinated to ligands having planar, aromatic subunits, we have recently reported a series of complexes containing modified phen/dppz ligands (phen = 1,10-phenanthroline and dppz = dipyrido[3,2-*a*:2′,3′-*c*]-phenazine). These new ligands have been designed so that besides containing the expansively aromatic "dppz" type of structure, they are also endowed with other electroactive subunits that impart special properties for the complexes in the presence of DNA.[18–21]

Some of the complexes containing a non-planar ligand also exhibit interesting properties upon binding to DNA,[22,23] It is well known that the five-membered imidazole ring is a component of the purine bases in DNA. Ji and co-workers have reported a series of imidazole-modified phen/bpy ligands where the imidazole ring is out of the plane of the phen moiety, and also biphenyl derivatives of phen/dppz, all of which help to explain the effect of ligand planarity on the DNA binding strength of the complexes.[24–28] The ancillary ligands of polypyridylruthenium(II) complexes have also been shown to have a significant effect on the spectral properties and the DNA-binding behavior of the complexes.[29–31] All the above studies revealed that modification of the ligands would lead to subtle or substantial changes in the binding modes, location, and affinities, and provide the chance to explore various valuable conformation- or site-specific DNA probes and potential chemotherapeutical agents. Thus, we focused on the construction of novel polypyridyl ligands containing fluorophores such as pyrene and anthracene in their imidazole architecture. This paper deals with the synthesis, characteri-

[a] School of Chemistry, University of Hyderabad
Hyderabad 500 046, India
Fax: +91-40-2301-2460
E-mail: tmmari@yahoo.com
[†] Deceased.

  DOI: 10.1002/ejic.200400952

zation, DNA binding, and photocleavage studies of the mixed-ligand Ru^{II} complexes $[Ru(phen)_2(aip)]^{2+}$ and $[Ru(phen)_2(pyip)]^{2+}$ containing ligands which have anthracene [viz. 2-(9-anthryl)-1*H*-imidazo[4,5-*f*][1,10]phenanthroline (aip)] or pyrene {viz. [2-(1-pyrenyl)-1*H*-imidazo[4,5-*f*][1,10]phenanthroline (pyip)} fluorophores in their architecture.

Results and Discussion

Synthesis and Characterization

The ligands aip and pyip were prepared by a method similar to that described by Steck and Day.[32] Condensation reactions of 1,10-phenanthroline-5,6-dione and 9-anthraldehyde or 1-pyrenecarboxaldehyde in the presence of ammonium acetate and glacial acetic acid produced aip and pyip, respectively. The corresponding ruthenium(II) complexes were synthesized by treating $[Ru(phen)_2Cl_2]\cdot 2H_2O$ with either aip or pyip (Figure 1). Each synthetic step involved here is straightforward and provides a good-to-moderate yield of the desired product in pure form. These products were characterized by elemental analysis, ^1H NMR, IR, luminescence, and UV/Vis spectroscopy, and MALDI-TOF mass spectrometry. The MALDI-TOF spectra show the base-peak at m/z = 396 for aip and at m/z = 420 for pyip. In the case of the corresponding mixed-ligand Ru^{II} complexes, peaks are seen at m/z = 1003 $[M - PF_6]^+$ and 858 $[M - 2\ PF_6]^+$ for $[Ru(phen)_2(aip)](PF_6)_2$ and similarly at m/z = 1026 $[M - PF_6]^+$ and 883 $[M - 2\ PF_6]^+$ for $[Ru(phen)_2(pyip)](PF_6)_2$, typical of PF_6 salts of polypyridylruthenium(II) complexes.[18–20,33]

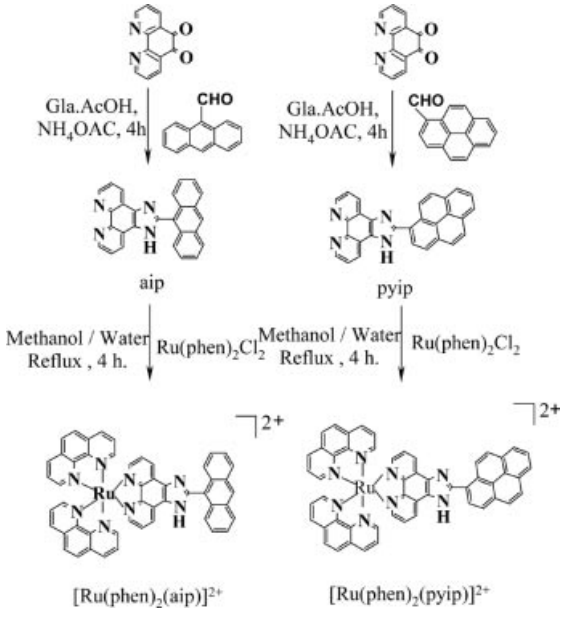

Figure 1. Scheme showing the synthesis of aip and pyip and their mixed-ligand ruthenium(II) complexes.

The ^1H NMR spectra of the two ligands (Figure 2) display a characteristic broad peak at δ = 14.20 (aip) and 13.73 ppm (pyip) for the N–H group of the imidazole ring.[27,28] In each of the two complexes, the signal of the proton on the nitrogen atom of the imidazole ring was not observed. Metal coordination causes electron deficiency in the ligand and, as a result, the imidazole proton becomes active and there is fast proton exchange between the two imidazole nitrogen atoms. Similar observations have been reported earlier.[27,28,34] In both complexes the signals of the *ortho*- and *para*-protons of the phenanthroline fragment of the ligands are shifted downfield and those of the *meta*-protons are shifted upfield compared to the free ligands. However, the proton signals of the anthracene and pyrene fragments of the ligands do not experience much shift compared to the free ligands. The other protons of both the complexes and the ligands give well-defined ^1H NMR spectra, which permit their unambiguous identification and assessment of purity.

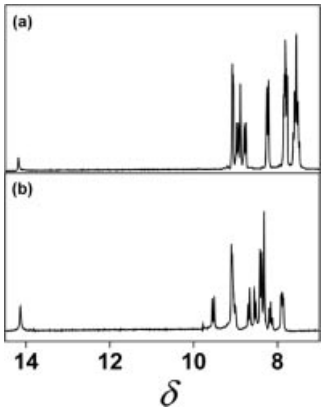

Figure 2. ^1H NMR spectra of (a) aip and (b) pyip in $CDCl_3$/CD_3OD and $[D_6]DMSO$.

The UV/Vis spectra of aip, pyip, and their ruthenium(II) complexes, along with the corresponding reference compounds synthesized during this study, are summarized in Table 1. The UV/Vis and luminescence spectra of both complexes are shown in Figure 3. As can be seen, the spectra of aip and pyip are characterized by low intensity but structured $\pi\rightarrow\pi^*$ transition absorption bands at 383 and 366 nm for aip and at 368 nm for pyip. These bands are ascribed to the anthracene and pyrene chromophores attached to the phenanthroline moiety.[35,36] The high-energy bands (aip: 251 nm; pyip: 234 and 280 nm) are attributed to the $\pi\rightarrow\pi^*$ transitions corresponding to the phenanthroline moiety of the ligands.

The low-energy bands at 452 (ε = 19675 $M^{-1}cm^{-1}$) and 457 nm (ε = 24066 $M^{-1}cm^{-1}$) are assigned as the MLCT $Ru(d\pi)\rightarrow aip/pyip(\pi^*)$ transitions for the complexes $[Ru(phen)_2(aip)]^{2+}$ and $[Ru(phen)_2(pyip)]^{2+}$, respectively, typical of any polypyridylruthenium(II) complex. The λ_{max} values of the MLCT transitions of these new complexes are bathochromically shifted in relation to the MLCT band of $[Ru(phen)_3]^{2+}$ (446 nm), with $[Ru(phen)_2(pyip)]^{2+}$ showing a higher red shift of 5 nm than $[Ru(phen)_2(aip)]^{2+}$ due to the extent of π delocalization of the chromophore. The bands centered at 254 and 264 nm are attributed to an in-

Table 1. UV/Vis and emission spectroscopic data.[a]

Compound	Absorbance[b] λ_{max} [nm] (log ε) Ligand transitions	MLCT	Emission[c] λ_{max} [nm] (φ)
phen	226 (4.71), 264 (4.55)	–	–
phen-dione	232 (3.82), 260 (3.81), 304 (3.64)	–	–
9-anthraldehyde	261 (4.29), 371 (3.15), 399 (3.16)	–	–
1-pyrenecarboxaldehyde	233 (4.70), 287 (4.57), 362 (4.44), 372 (4.42), 394 (4.33)	–	–
aip	251(4.94), 366 (3.89), 383 (3.88)	–	447, 535 (0.81)
pyip	234 (4.71), 280 (4.52), 368 (4.44)	–	411, 443, 494 (0.63)
$[Ru(phen)_3](PF_6)_2$	223 (4.93), 263 (5.07), 422 (4.25)	446 (4.28)	596 (0.028)
$[Ru(phen)_2(aip)](PF_6)_2$	221 (4.96), 254 (5.22), 385 (4.30)	452 (4.29)	604 (0.005)
$[Ru(phen)_2(pyip)](PF_6)_2$	376 (4.64); 264 (5.08); 225 (5.00)	457 (4.38)	601 (0.0006)

[a] Spectra were recorded in CH_3CN. [b] Error limits: λ_{max}: ±1 nm; log ε: ±10%. [c] Error limits: λ_{em}: ±1 nm; φ: ±10%.

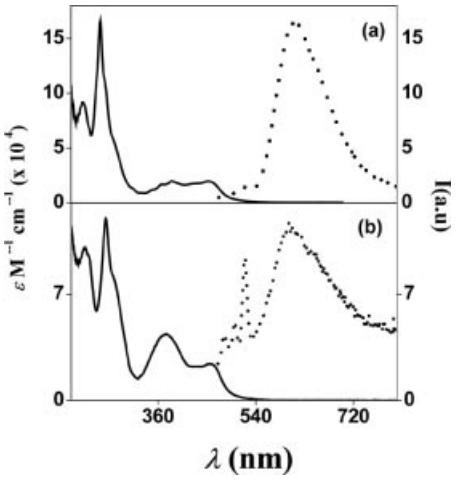

Figure 3. UV/Vis (– – –) and luminescence (·····) spectra of $[Ru(phen)_2(aip)]^{2+}$ (a) and $[Ru(phen)_2(pyip)]^{2+}$ (b) in CH_3CN.

traligand (IL) π→π* transition for $[Ru(phen)_2(aip)]^{2+}$ and $[Ru(phen)_2(pyip)]^{2+}$, respectively.

When aip is excited at 360 nm, the emission maximum appears at 535 nm (φ = 0.81 in CH_3CN). In the case of pyip (excited at 330 nm), the emission maximum appears at 494 nm (φ = 0.63 in CH_3CN). The steady-state and time-resolved absorption and fluorescence spectroscopic properties of aip, which is a bichromophoric molecule, reveal that a rapid and efficient intra-EET process dominates its excited-state relaxation dynamics in solution.[37] $[Ru(phen)_2(aip)]^{2+}$ and $[Ru(phen)_2(pyip)]^{2+}$ show an emission band centered at 604 and 601 nm with quantum yields of 0.005 and 0.0006, respectively in CH_3CN (λ_{exc} = 450 nm; see Figure 3). The origin of the spike at around 520 nm in the emission spectrum (Figure 3b) is due to Raman scattering. Since $[Ru(phen)_2(pyip)]^{2+}$ is weakly fluorescent and the gain of the instrument has to be increased to compensate for the low quantum yield (φ = 0.0006 in CH_3CN), the Raman scatter becomes visible. For highly fluorescent $[Ru(phen)_2(aip)]^{2+}$ (φ = 0. 005 in CH_3CN), the emission spectra overwhelms the Raman peak and thus it is not observed. The spectral shape and the λ_{em} values are quite similar to those of $[Ru(phen)_2(dppz)]^{2+}$, the ^{3}MLCT emission band maximum of which has been reported to be located at 618 nm.[17] The emission quantum yields of the complexes (Table 1) investigated here are lower than that of $[Ru(phen)_3]^{2+}$ (φ = 0.028 in CH_3CN)[38] and the order is $[Ru(phen)_3]^{2+}$ > $[Ru(phen)_2(aip)]^{2+}$ >> $[Ru(phen)_2(pyip)]^{2+}$.

Electrochemistry

During the cathodic scans in the cyclic voltammetric experiments, carried out in DMF containing 0.1 M TBAP, ligands aip and pyip show reversible (i_{pc}/i_{pa} = 0.9–1.0) and diffusion-controlled [$i_{pc}/v^{1/2}$ is constant in the scan-rate (v) range 50–500 mV s^{-1}] one-electron transfer (ΔE_P = 60–70 mV; ΔE_P = 65 ± 3 mV for the Fc^+/Fc couple)[39] responses at –1.48 and –1.46 V (vs. SCE), respectively. These potentials are close to those observed for the one-electron reductions of phen-dione (–1.47 V). The second reduction step appears as either quasi-reversible (i_{pc}/i_{pa} = 0.2–0.7 and ΔE_P = 90–200 mV at a scan rate over the range of 100–500 mV s^{-1}) or totally irreversible responses for aip and pyip at –1.61 and –1.64 V, respectively. The oxidation of pyip occurs at +1.42 V, whereas for aip it occurs at +1.38 V. The oxidation potential shifts more positively for pyip than for aip due to the greater π-delocalized nature of the pyrene moiety in the case of pyip when compared to anthracene in aip.

The cyclic and differential-pulse voltammograms of the two new complexes are compared with that of $[Ru(phen)_3]^{2+}$ in Figure 4. Each complex exhibits well-shaped oxidation and reduction waves in the sweep range from –2.0 to +1.6 V vs. SCE containing 0.1 M TBAP. The complex $[Ru(phen)_2(aip)]^{2+}$ exhibits a well-shaped reversible oxidation wave (+1.43 V) in acetonitrile and three reduction waves –1.29, –1.49, and –1.96 V in DMF. The first two reduction waves are reversible and the last one at –1.96 V is a poorly shaped quasi-reversible wave. For $[Ru(phen)_2(pyip)]^{2+}$, a reversible oxidation wave at +1.47 V in acetonitrile and two reversible reduction waves at –1.21 and –1.43 V in DMF are observed. The redox potential data for all the above compounds as measured by the cyclic and differential-pulse voltammetric method are summarized in Table 2.

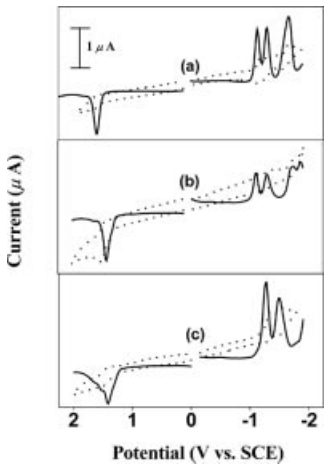

Figure 4. Cyclic (·····) and differential-pulse (−) voltammograms of (a) $[Ru(phen)_3]^{2+}$, (b) $[Ru(phen)_2(aip)]^{2+}$, and (c) $[Ru(phen)_2(pyip)]^{2+}$. CH_3CN and DMF containing 0.1 M TBAP were used as solvents for the anodic and cathodic runs, respectively. Scan rate: 100 mV s^{-1}.

Table 2. Redox potential data.[a]

Compound	Oxidation, $E_{1/2}$ (V vs. SCE)	Reduction, $E_{1/2}$ (V vs. SCE)
phen	–	–1.92[d]
phen-dione	–	–0.45, –1.08[c]
9-anthraldehyde	+1.67[b]	–1.12[d]
pyrene	+1.49[c]	–
1-pyrenecarboxaldehyde	+1.64[b]	–1.27[d]
aip	+1.38[b]	–1.48, –1.61[d]
pyip	+1.42[b]	–1.46, –1.64[d]
$[Ru(phen)_3](PF_6)_2$	+1.37[c]	–1.19, –1.34, –1.69[d]
$[Ru(phen)_2(dppz)](PF_6)_2$	+1.41[c]	–0.82, –1.25, –1.47[d]
$[Ru(phen)_2(aip)](PF_6)_2$	+1.43[c]	–1.29, –1.49, –1.96[d]
$[Ru(phen)_2(pyip)](PF_6)_2$	+1.47[c]	–1.21, –1.43[d]

[a] Obtained from the differential-pulse voltammetric measurements. Error limits: $E_{1/2}$: ±0.03 V. [b] CH_2Cl_2, 0.1 M TBAP. [c] CH_3CN, 0.1 M TBAP. [d] DMF, 0.1 M TBAP.

Oxidation of the complexes involves removal of an electron from the dπ orbital of Ru^{II}, while reduction involves transfer of an electron to the ligand-centered orbitals.[28] As expected, the oxidation potential of $[Ru(phen)_2(pyip)]^{2+}$ is 40 mV more positive than $[Ru(phen)_2(aip)]^{2+}$. The attachment of a pyrene ring (extended hydrophobicity/aromaticity) to the IP (imidazophenanthroline) moiety expands the π delocalization and thus decreases the σ-donor capacity of pyip, which leads to a decrease in the electron density on the Ru^{II} ion and, in turn, stabilizes the metal π (t_{2g}) orbital.[40] As a result, the oxidation potential shifts positively for $[Ru(phen)_2(pyip)]^{2+}$ when compared to $[Ru(phen)_2(aip)]^{2+}$. The first reduction in both the complexes is expected to be centered at aip/pyip because of the availability of the most stable LUMO.[41] The other reductions observed for both complexes are characteristic of the ancillary phen ligands.[42] Thus, in the case of $[Ru(phen)_2(aip)]^{2+}$, reductions at –1.29, –1.49, and –1.96 V are assigned to aip/$aip^{\cdot-}$, $phen_1/phen_1^{\cdot-}$, and $phen_2/phen_2^{\cdot-}$ couples, respectively. For $[Ru(phen)_2(pyip)]^{2+}$, the reductions at –1.21 and –1.43 V are assigned to pyip/$pyip^{\cdot-}$ and $phen_1/phen_1^{\cdot-}$ processes, respectively; the second reduction associated with $phen_2$ could not be observed.

DNA-Binding Experiments

Binding of the chloride salts of the two Ru^{II} complexes synthesized in this study with CT DNA were monitored by absorption, luminescence, thermal denaturation, and viscosity methods, and the results are summarized in this section, which also discusses aspects related to the ability of these complexes to act as "molecular light switches" for DNA.

Absorption Titration

Both $[Ru(phen)_2(aip)]^{2+}$ and $[Ru(phen)_2(pyip)]^{2+}$ were titrated with CT DNA. The change in the spectral profiles during titration is shown in Figure 5a and b. As the DNA concentration is increased, $[Ru(phen)_2(aip)]^{2+}$ and $[Ru(phen)_2(pyip)]^{2+}$ show hypochromicity (39% and 61%,) and isosbestic points (482 and 496 nm), along with bathochromic shifts of 6 and 9 nm, respectively. To compare quantitatively the affinity of the two complexes towards

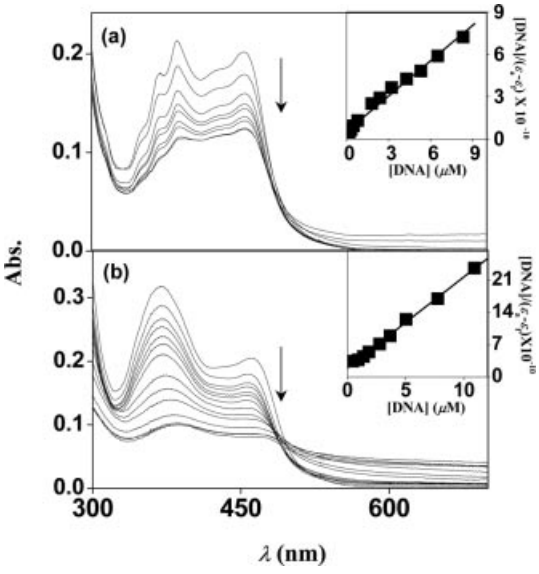

Figure 5. UV/Vis spectra of (a) $[Ru(phen)_2(aip)]^{2+}$ (5 μM) and (b) $[Ru(phen)_2(pyip)]^{2+}$ (5 μM) in the absence (top curve) and presence (subsequent curves) of increasing concentrations (0–100 μM) of CT DNA in buffer A. The inset graph shows a fit of the absorbance data used to obtain the binding constant.[56]

Table 3. Results of absorption titration and thermal melting experiments.[a]

Compound	K_b [M^{-1}]	T_m [°C] (σ_T)
DNA	–	61 (19)
$[Ru(phen)_3]^{2+}$	8.24×10^3	62 (21)
$[Ru(phen)_2(aip)]^{2+}$	1.01×10^6	64 (28)
$[Ru(phen)_2(pyip)]^{2+}$	1.57×10^6	65 (25)
$[Ru(phen)_2(dppz)]^{2+}$	$>10^7$	65 (26)

[a] Error limits: K_b: ±10%; T_m: ±1 °C; σ_T: ±1°.

DNA, the intrinsic binding-constant values (K_b) were determined by monitoring the absorbance at the MLCT band position and were found to be as high as $1.01 \pm 0.1 \times 10^6$ and $1.57 \pm 0.8 \times 10^6$ M^{-1} for $[Ru(phen)_2(aip)]^{2+}$and $[Ru(phen)_2(pyip)]^{2+}$, respectively (Table 3). The extent of hypochromism commonly parallels the intercalative strength of the ligand and, moreover, a higher planar area, an extended π system, hydrophobicity, and aromaticity lead to deep penetration and hence more stacking within the base-pairs of DNA. Thus, the intercalative strength follows the order $[Ru(phen)_2(dppz)]^{2+} \approx [Ru(ip)_2(dppz)]^{2+} \geq [Ru(phen)_2(pyip)]^{2+} > [Ru(phen)_2(aip)]^{2+} > [Ru(phen)_3]^{2+}$ (ip = imidazo[4,5-*f*][1,10]phenanthroline).[29]

Luminescence Titration

The steady-state emission spectra of 7 μM solutions of $[Ru(phen)_2(aip)]^{2+}$ and $[Ru(phen)_2(pyip)]^{2+}$ in Tris buffer (5 mM Tris, 50 mM NaCl, pH = 7.1) show an increase in the emission intensity with successive addition of CT DNA. In the case of $[Ru(phen)_2(aip)]^{2+}$, the emission maximum at 604 nm due to the ^{3}MLCT [dπ(Ru)→π*(aip)][38] state increases initially at low [DNA nucleotide phosphate]/[Ru] ratio, but reaches a plateau, with an apparent enhancement factor of about 5, at a higher [DNA nucleotide phosphate]/[Ru] ratio of 27. The complex has an appreciable emission in the buffer in the absence of DNA and shows a marginal red-shift of 2 nm on addition of DNA (Figure 6a). The luminescence due to $[Ru(phen)_2(pyip)]^{2+}$ at 601 nm is assigned as a ^{3}MLCT [dπ(Ru)→π*(pyip)] state, and increases steadily with increasing addition of CT DNA, reaching a maximum (approx. 9 times) at a [DNA nucleotide phosphate]/[Ru] ratio of 43 (see Figure 6b). The complex has very weak emission in the aqueous medium in the absence of DNA, but on addition of increasing amounts of DNA the emission intensity increases with a bathochromic shift of about 4 nm. The emission enhancement of both complexes in the presence of DNA is much smaller than that observed for the dppz-based polypyridylruthenium(II) intercalators reported by Barton et al.[10,15,17] The shielding of the nitrogen atoms on the intercalating ligands, especially the imidazole nitrogen atoms, from protonation in the bulk solvent medium causes an emission enhancement, which has been extensively characterized and described as a "molecular light switch".[10,15,17] The mobility of these complexes is restricted at the binding site and so the vibrational modes of relaxation (collision and energy dissipation) decrease on intercalation.[28] The binding constants obtained are reasonably well in agreement with the values from the absorption titration experiment. The binding site sizes (n) for $[Ru(phen)_2(aip)]^{2+}$ and $Ru(phen)_2(pyip)]^{2+}$ are evaluated as 2 and 3.

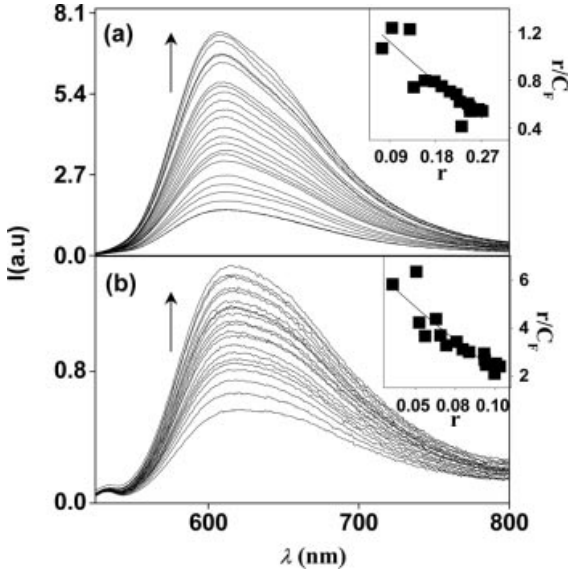

Figure 6. Luminescence spectra of (a) $[Ru(phen)_2(aip)]^{2+}$ (7 μM) and (b) $[Ru(phen)_2(pyip)]^{2+}$ (7 μM) in the absence (bottom curve) and presence (subsequent curves) of increasing concentrations (0–300 μM) of CT DNA in buffer A (λ_{exc} = 450 nm). The inset graph shows a fit of the emission data to Equation (4).

DNA Melting Experiments

Other strong evidence for the intercalation of both the complexes into the helix was obtained from the DNA melting studies. Intercalation of small molecules into the double helix is known to increase the helix melting temperature (T_m), the temperature at which the double helix denatures into single-stranded DNA.[43] The extinction coefficient of DNA bases at 260 nm in the double-helical form is much less than in the single-stranded form; hence, melting of the helix leads to an increase in the absorption[44] at this wavelength. CT DNA was seen to melt at 61 ± 1 °C (2 mM NaCl, 1 mM phosphate) in the absence of any added complex. The T_m of DNA is increased by 4 and 5 °C in the presence of $[Ru(phen)_2(aip)]^{2+}$ and $[Ru(phen)_2(pyip)]^{2+}$ (at [DNA nucleotide phosphate]/[complex] = 25), respectively. The DNA melting curves in the absence and in the presence of both complexes are presented in Figure 7 and the T_m and the σ_T values of CT DNA in the absence and presence of the

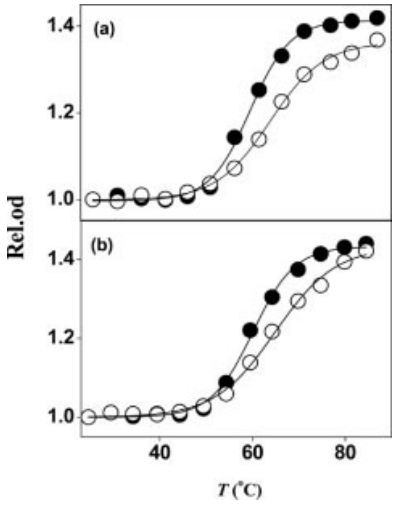

Figure 7. Melting curves for CT DNA in the absence (filled circles) and in the presence (open circles) of $[Ru(phen)_2(aip)]^{2+}$ (a) and $[Ru(phen)_2(pyip)]^{2+}$ (b) in buffer B.

complexes are tabulated in Table 3. These establish the increased stability of the double helix when $[Ru(phen)_2(aip)]^{2+}$ and $[Ru(phen)_2(pyip)]^{2+}$ bind to DNA. The increases in the melting temperatures are comparable to the values observed with the classical intercalator ethidium and lend strong support for intercalation into the helix.[44,45]

Viscometric Titration

Intercalation of a ligand into DNA is known to cause a significant increase in the viscosity of a DNA solution due to an increase in the separation of the base pairs at the intercalation site and, hence, an increase in the overall DNA molecular length (contour length). In contrast, a ligand that binds in the DNA grooves causes a less-pronounced change (positive or negative) or no change in the viscosity of a DNA solution.[46] The effects of $[Ru(phen)_2(aip)]^{2+}$, $[Ru(phen)_2(pyip)]^{2+}$, ethidium bromide (EtBr), and $[Ru(phen)_3]^{2+}$ on the viscosity of CT DNA solution were studied in order to assess the binding mode of these complexes with DNA. Plots of $(\eta/\eta_o)^{1/3}$ vs. [Drug]/[DNA] are shown in Figure 8. The viscosity of DNA bound with $[Ru(phen)_2(aip)]^{2+}$, $[Ru(phen)_2(pyip)]^{2+}$, and EtBr increases dramatically, thus indicating that both complexes, as well as the classical intercalator EB, intercalate the base pairs of DNA and that $[Ru(phen)_2(pyip)]^{2+}$ has a slightly stronger binding affinity than $[Ru(phen)_2(aip)]^{2+}$**.** However, addition of $[Ru(phen)_3]^{2+}$ has no effect on the DNA viscosity, as reported previously.[46]

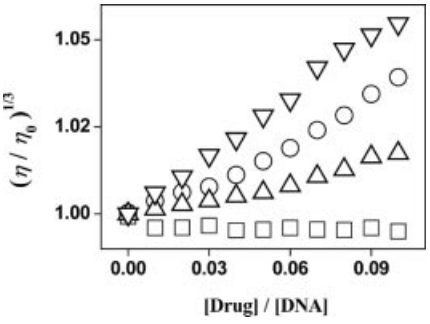

Figure 8. Results of viscometric titrations carried out for CT DNA (300 μM) in the presence of $[Ru(phen)_3]^{2+}$ (squares), $[Ru(phen)_2(aip)]^{2+}$ (triangles, tip up), $[Ru(phen)_2(pyip)]^{2+}$ (open circles) and EB (triangles, tip down) in buffer C.

DNA Photocleavage

When circular plasmid DNA is subjected to electrophoresis relatively fast migration is observed for the supercoiled form (form I), whereas if scission occurs on one strand (nicking), the supercoils will relax to generate a slower moving open circular form (form II). DNA photocleavage experiments were carried out with both the complexes and with $[Ru(phen)_3]^{2+}$ (for comparison). Figure 9 summarizes the results. Control runs in the agarose-gel electrophoresis experiments suggested that untreated pBR 322 DNA does not show any cleavage in the dark, and even upon irradiation with a 450 ± 5 nm light (compare lanes 1 and 2; Figure 9). Lower activity was observed for pBR 322 treated with $[Ru(phen)_2(aip)]^{2+}$, $[Ru(phen)_2(pyip)]^{2+}$, and $[Ru(phen)_3]^{2+}$ in the dark experiments (lanes 3, 5, and 7; Figure 9). After irradiation for 60 min (see lanes 4, 6, and 8; Figure 9) single-strand nicking is observed, and the percentage of conversion from form I to form II was calculated with Equation (5) (see Exp. Sect.). Based on the percentage conversion from form I to form II for these complexes, DNA-nicking efficiencies were seen to roughly follow the trend $[Ru(phen)_2(pyip)]Cl_2$ > $[Ru(phen)_2(aip)]Cl_2$ > $[Ru(phen)_3]Cl_2$. These can be explained on the basis of the binding nature of the intercalating ligands in the complexes due to the extended π-aromatic nature in the case of pyip when compared to aip. The photocleavage efficiencies of these complexes are similar to those of $[Ru(bpy)_2(ip)]^{2+}$ and $[Ru(bpy)_2(pip)]^{2+}$ (ip = imidazo[4,5-*f*][1,10]phenanthroline; pip = 2-phenylimidazo[4,5-*f*][1,10]phenanthroline) reported in the literature.[28]

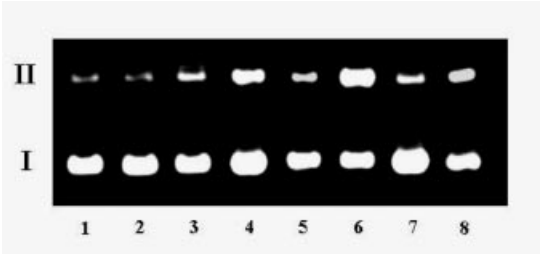

Figure 9. Light-induced nuclease activities of the investigated ruthenium(II) complexes. Dark and light experiments: lanes 1 and 2: untreated pBR 322 (100 μM) in the dark and upon irradiation. Lanes 3, 5, and 7: pBR 322 + $[Ru(phen)_2(aip)]^{2+}$, $[Ru(phen)_2(pyip)]^{2+}$, and $[Ru(phen)_3]^{2+}$ respectively (10 μM) in the dark. Lanes 4, 6, and 8: pBR 322 + $[Ru(phen)_2(aip)]^{2+}$, $[Ru(phen)_2(pyip)]^{2+}$, and $[Ru(phen)_3]^{2+}$, respectively, upon irradiation. λ_{irr} = 450 ± 5 nm (60 min) in each case.

In attempts to unravel the probable DNA photocleavage mechanism of these new complexes, a few control experiments were conducted in the presence of various "inhibitors". Photocleavage by $[Ru(phen)_3]Cl_2$ has been reported[47] to involve a $^1O_2$-based mechanism. In the case of $[Ru(phen)_2(aip)]^{2+}$ (see Figure 10), irradiation for 60 min in the presence of DABCO (lane 5; a $^1O_2$ "quencher") or Tiron (lane 7; a superoxide anion radical quencher) does not affect the photocleavage mechanism. Purging the reaction mixture with N_2 (lane 3) for 15 min to remove O_2 was also found not to inhibit the photocleavage mechanism. Inhibition was seen in the presence of DMSO (lane 4) and manni-

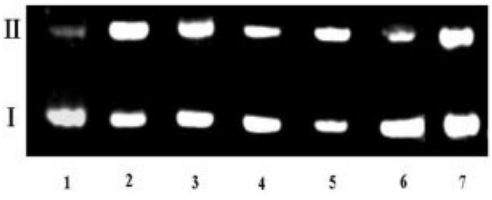

Figure 10. Effect of "inhibitors" on the light-induced nuclease activity of $[Ru(phen)_2(aip)]^{2+}$. Lanes 1 and 2: pBR 322 and $[Ru(phen)_2(aip)]^{2+}$. Lanes 3–7: pBR 322 + $[Ru(phen)_2(aip)]^{2+}$ in the presence of N_2, DMSO (200 mM), DABCO (10 mM), mannitol (100 mM), and Tiron (10 mM), respectively, upon irradiation for 60 min at 450 ± 5 nm in each case.

tol (lane 6), and mannitol is a better inhibitor than DMSO. Both DMSO and mannitol are scavengers of hydroxyl radicals.

In the case of $[Ru(phen)_2(pyip)]^{2+}$ (Figure 11), moderate activity was still observed in the presence of DABCO (lane 5) and DMSO (lane 4), whereas no effect was observed with N_2 (lane 3) or Tiron (lane 7). However, the activity is inhibited very strongly in the presence of mannitol (lane 6). These results suggest that the reactive oxygen species ·OH and singlet oxygen (to a lesser extent) play a significant role in the cleavage mechanism for $[Ru(phen)_2(pyip)]Cl_2$, whereas for $[Ru(phen)_2(aip)]Cl_2$ only the hydroxyl radical plays a role in the photocleavage mechanism.[48]

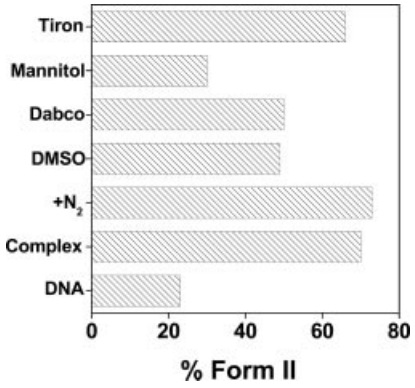

Figure 11. Bar diagram representation of the effect of "inhibitors" on the light-induced nuclease activity of $[Ru(phen)_2(pyip)]^{2+}$. Lanes 1 and 2: pBR 322 and $[Ru(phen)_2(pyip)]^{2+}$. Lanes 3–7: pBR 322 + $[Ru(phen)_2(pyip)]^{2+}$ in the presence of N_2, DMSO (200 mM), DABCO (10 mM), mannitol (100 mM), and Tiron (10 mM), respectively, upon irradiation for 60 min at 450 ± 5 nm in each case.

Conclusions

Two new anthracene/pyrene chromophore-appended polypyridyl ligands (aip and pyip), and their mixed-ligand ruthenium(II) complexes $[Ru(phen)_2(aip)]^{2+}$ and $[Ru(phen)_2(pyip)]^{2+}$, have been synthesized and fully characterized by spectroscopic and electrochemical methods. Studies with DNA have revealed that these complexes bind to DNA, mainly in an intercalative mode, with moderate strengths. The observation that $[Ru(phen)_2(pyip)]^{2+}$ binds DNA more strongly than $[Ru(phen)_2(aip)]^{2+}$ suggests that the increased surface area available for stacking by this complex within the duplex leads to a substantial increase in its intercalative binding affinity. In accordance with this interpretation, $[Ru(phen)_2(pyip)]^{2+}$ is found to be a better "molecular light switch" for DNA than $[Ru(phen)_2(aip)]^{2+}$. The photonuclease activity is also higher for $[Ru(phen)_2(pyip)]^{2+}$ than $[Ru(phen)_2(aip)]^{2+}$ and is comparable to that of $[Ru(bpy)_2(ip)]^{2+}$ and $[Ru(phen)_3]^{2+}$. Moreover, the reactive oxygen species ·OH plays a significant role in the cleavage mechanism of both $[Ru(phen)_2(pyip)]Cl_2$ and $[Ru(phen)_2(aip)]Cl_2$. Studies carried out so far have revealed that modification of phen, especially extension of the planarity of the ligand and attaching aromatic chromophores to it, will increase the strength of interaction of its complexes with DNA.

Experimental Section

Materials: All common chemicals and solvents utilized in this study were obtained in their highest available purity from B.D.H (Mumbai, India). Ruthenium trichloride hydrate, tetrabutylammonium perchlorate (TBAP), and tetrabutylammonium chloride (TBACl) were obtained from Aldrich Chemical Co. (USA). Pyrene, 1-pyrenecarboxaldehyde, 9-anthraldehyde, the deuterated solvents, and the calf-thymus DNA (CT DNA) were also purchased from Aldrich. Agarose (molecular biology grade) and ethidium bromide were purchased from Bio-Rad Laboratories Inc. (USA). Supercoiled pBR 322 DNA (CsCl purified) was obtained from Bangalore Genie (Bangalore, India) and was used as received. All the solvents utilized for spectroscopic and electrochemical work were rigorously purified before use according to standard procedures.[49] Deionized, triply distilled water was used for preparing various buffers. 1,10-phenanthroline-5,6-dione,[50] and $[Ru(phen)_2Cl_2]\cdot 2H_2O$,[51] were synthesized by applying the reported procedures.

2-(9-Anthryl)-1*H*-imidazo[4,5-*f*][1,10]phenanthroline (aip): A mixture of phen-dione (0.53 g, 2.50 mmol), 9-anthraldehyde (0.72 g, 3.50 mmol), ammonium acetate (3.88 g, 50.00 mmol), and glacial acetic acid (15 mL) was refluxed for 4 h and then cooled to room temperature. It was diluted with water and dropwise addition of concentrated aqueous ammonia gave a yellow precipitate, which was collected, washed with water, and dried. The crude product obtained was purified by recrystallization from $CHCl_3$/MeOH (4:1, v/v) and dried. Yield: 0.71 g (72%). $C_{27}H_{16}N_4$ (396.45): calcd. C 81.70, H 4.04, N 14.13; found C 81.63, H 4.11, N 14.19. MALDI-TOF: *m*/*z* = 396 $[M]^+$. IR (KBr): $\tilde{\nu}$ = 3441 (N–H), 1604 (C=N) cm^{-1}. ^1H NMR ([D$_6$]DMSO, 200 MHz, TMS): δ = 14.20 (s, 1 H), 9.09 (dd, J_1 = 2, J_2 = 3 Hz, 2 H), 8.94 (dd, J_1 = 2, J_2 = 6 Hz, 2 H), 8.80 (d, J = 7.8 Hz, 1 H), 8.26 (d, J = 7.8 Hz, 2 H), 7.84 (m, 4 H), 7.57 (m, 4 H) ppm.

2-(1-Pyrenyl)-1*H*-imidazo[4,5-*f*][1,10]phenanthroline (pyip): A mixture of phen-dione (0.53 g, 2.50 mmol), 1-pyrenecarboxaldehyde (0.81 g, 3.50 mmol), ammonium acetate (3.88 g, 50.00 mmol), and glacial acetic acid (15 mL) was refluxed for 4 h The above solution was cooled to room temperature and diluted with water. Dropwise addition of concentrated aqueous ammonia gave a yellow precipitate, which was collected, washed with water, and dried. The crude product thus obtained was purified by recrystallization from pyridine/water (9:1, v/v) and dried. Yield: 0.71 g (68%). $C_{29}H_{16}N_4$ (420.48): calcd. C 82.77, H 3.81, N 13.32; found C 82.81, H 3.74, N 13.39. MALDI-TOF: *m*/*z* = 420 $[M]^+$. IR (KBr): $\tilde{\nu}$ = 3426 (N–H), 1602 (C=N) cm^{-1}. ^1H NMR ($CDCl_3$/[D$_6$]DMSO, 200 MHz, TMS): δ = 13.73 (s, 1 H), 9.28 (d, J = 9.8 Hz, 1 H), 9.12 (dd, J_1 = 5, J_2 = 6 Hz, 2 H), 8.93 (d, J = 8 Hz, 1 H), 8.52 (d, J = 8.8 Hz, 1 H), 8.18 (m, 8 H), 7.66 (dd, J_1 = 3.4, J_2 = 3.4 Hz, 2 H) ppm.

{2-(9-Anthryl)-1*H*-imidazo[4,5-*f*][1,10]phenanthroline}bis(1,10-phenanthroline)ruthenium(II) Bis(hexafluorophosphate) Dihydrate $[Ru(phen)_2(aip)](PF_6)_2\cdot 2H_2O$: This complex was prepared by refluxing aip (0.30 g, 0.76 mmol) with $[Ru(phen)_2Cl_2]\cdot 2H_2O$ (0.43 g, 0.75 mmol) in CH_3OH/H_2O (1:1, v/v) for 4 h. The resulting solution was cooled to room temperature, then 15 mL of water was added and the mixture filtered. Addition of a saturated solution of NH_4PF_6 to the filtrate precipitated bright orange-red crude $[Ru(phen)_2(aip)](PF_6)_2$, which was purified by column chromatography [alumina and acetonitrile/toluene (3:2, v/v)] and further recrystallized from acetone/diethyl ether (1:5, v/v). Yield: 0.48 g (54%). $C_{51}H_{36}F_{12}N_8O_2P_2Ru$ (1183.9): calcd. C 51.71, H 3.04, N 9.46; found C 51.86, H 2.98, N 9.53. MALDI-TOF: *m*/*z* = 1003 $[M - PF_6]^+$, 858 $[M - 2\ PF_6]^+$. IR (KBr): $\tilde{\nu}$ = 3381 (N–H), 1601 (C=N), 837 (PF_6) cm^{-1}. ^1H NMR ([D$_6$]DMSO, 200 MHz, TMS):

δ = 8.97 (d, J = 7.5 Hz, 1 H), 8.81 (m, 4 H), 8.42 (s, 4 H), 8.26 (m, 4 H), 8.09 (m, 5 H), 7.82 (m, 9 H), 7.61 (m, 4 H) ppm.

Bis(1,10-phenanthroline){2-(1-pyrenyl)-1*H*-imidazo[4,5-*f*][1,10]phenanthroline}ruthenium(II) Bis(hexafluorophosphate) Dihydrate [Ru(phen)$_2$(pyip)](PF$_6$)$_2$·2H$_2$O: This mixed-ligand Ru^{II} complex was prepared by refluxing pyip (0.34 g, 0.82 mmol) with [Ru(phen)$_2$Cl$_2$]·2H$_2$O (0.45 g, 0.80 mmol) in CH$_3$OH/H$_2$O (1:1, v/v) for 4 h. The crude bright orange-red [Ru(phen)$_2$(pyip)](PF$_6$)$_2$ was obtained upon adding a saturated solution of NH$_4$PF$_6$. It was purified by column chromatography [alumina, acetonitrile/toluene (3:2, v/v)] and further recrystallized from acetone/diethyl ether (1:5, v/v). Yield: 0.49 g (53%). C$_{53}$H$_{36}$F$_{12}$N$_8$O$_2$P$_2$Ru (1207.9): calcd. C 52.67, H 2.98, N 9.28; found C 52.78, H 3.06, N 9.19. MALDI-TOF: m/z = 1026 [M – PF$_6$]$^+$, 883 [M – 2 PF$_6$]$^+$. IR (KBr): $\tilde{\nu}$ = 3377 (N–H), 1599 (C=N), 837 (PF$_6$) cm^{-1}. ^{1}H NMR ([D$_6$]DMSO, 200 MHz, TMS): δ = 9.43 (d, J = 10 Hz, 1 H), 9.19 (d, J = 7.6 Hz, 2 H), 8.80 (m, 4 H), 8.69 (d, J = 7.8 Hz, 1 H), 8.58 (d, J = 8.8 Hz, 1 H), 8.43 (m, 8 H), 8.15 (m, 6 H), 7.82 (m, 6 H), 7.20 (m, 2 H) ppm.

The hexafluorophosphate salts of the complexes were converted into the water-soluble chloride salts by treating the former salt solutions with an excess of TBACl in acetone. The chloride salts, which are insoluble in acetone, instantaneously precipitated from the solution. They were filtered and vacuum-dried before use. The yield was about 90% of the theoretical value in each case.

Spectroscopy and Electrochemistry: Care was taken to avoid the entry of direct, ambient light into the samples in all the spectroscopic and electrochemical experiments described below. Unless otherwise specified, all the experiments were carried out at 293 ± 3 K. Elemental analyses were performed with a Flash EA 1112 series CHNS (Thermo Finnigan/Eager 300) analyzer. Acetanilide was used as the reference standard. Mass (MALDI-TOF) spectra were recorded with a Kompact MALDI 4 mass spectrometer (Kratos Analytical Ltd.). The instrument was operated in reflection time-of-flight mode with an accelerating potential of 20 kV and in the negative ion recording mode. The IR spectra were recorded with a Jasco Model 5300 FT-IR spectrophotometer. The spectra of the solid samples were recorded by dispersing the samples as KBr pellets. The ^{1}H NMR spectra were recorded with a Bruker NR-200 AF-FT NMR spectrometer, with CDCl$_3$ or [D$_6$]-DMSO as the solvent and tetramethylsilane (TMS) as the internal standard. The UV/Vis spectra were recorded with a Shimadzu model UV-3101 spectrophotometer. A matched pair of quartz cuvettes (path length 1 cm) was employed. Steady-state fluorescence spectra were recorded with a Spex Fluoromax-3 spectrophotometer using a 1-cm quartz cell. Detection of emission was done at right angles to the incident beam. The excitation and emission slit widths employed were, typically, 5 nm. While hexafluorophosphate salts of the complexes were employed for the luminescence measurements in nonaqueous solvents (rigorously dried CH$_2$Cl$_2$, THF, 1,4-dioxane, CH$_3$CN, and DMF), the corresponding chloride salts were used for measurements in aqueous and aqueous buffered solutions. The optical densities of the samples were adjusted to ≤0.2 at the excitation wavelength in each case. Emission quantum yields (φ) were estimated by integrating the area under the fluorescence curves and by using the formula given in Equation (1),[52] where A is the area under the emission spectral curve and OD is the optical density of the compound at the excitation wavelength. 1,6-Diphenyl-1,3,5-hexatriene (dpht, φ = 0.80 in cyclohexane)[53] was used as the standard for the calculation of the quantum yield values of the new ligands aip and pyip. The standard used for emission quantum yield measurements for the ruthenium(II) complexes was [Ru(phen)$_3$](PF$_6$)$_2$ (φ = 0.028 in CH$_3$CN).[38] Refractive index corrections were incorporated when reporting the emission data in various solvents.[54]

$$\phi_{sample} = \frac{OD_{standard} \times A_{sample}}{OD_{sample} \times A_{standard}} \times \phi_{standard} \quad (1)$$

Cyclic and differential-pulse voltammetric experiments (CH$_3$CN/DMF/CH$_2$Cl$_2$, 0.1 M TBAP) were performed with a CH Instruments model CHI 620A electrochemical analyzer (working and auxiliary electrodes: Pt; reference electrode: SCE). The Fc$^+$/Fc (Fc = ferrocene) couple was used to calibrate the redox potential values.

DNA-Binding and Photocleavage Studies: The concentration of CT DNA was calculated from its known extinction coefficient at 260 nm (6600 M^{-1} cm^{-1}).[55] Unless otherwise specified, the concentration of DNA is expressed in base pairs (BP) throughout this manuscript. Buffer A (5 mM Tris, 50 mM NaCl, pH = 7.1), buffer B (1 mM phosphate, 2 mM NaCl, pH = 7.0), and buffer C (1.5 mM Na$_2$HPO$_4$, 0.5 mM NaH$_2$PO$_4$, 0.25 mM Na$_2$EDTA, pH = 7.0) were used for absorption and luminescence titration, thermal denaturation, and viscometric experiments, respectively. TAE (tris-acetate ethylenediaminetetraacetate) 1X buffer was used for gel electrophoresis cleavage and inhibition experiments. Absorption titration experiments were performed by maintaining a constant metal complex concentration (5 μM) and varying the nucleic acid concentration (0–100 μM). After the addition of DNA to the metal complex, the resulting solution was allowed to equilibrate at 25 °C for 10 min, after which the absorption readings were noted. The data were then fit to Equation (2) to obtain the intrinsic binding constant K_b,[56] where ε_a, ε_f, and ε_b are the apparent, free, and bound metal complex extinction coefficients, respectively.

$$[DNA]/(\varepsilon_a - \varepsilon_f) = [DNA]/(\varepsilon_b - \varepsilon_f) + 1/K_b(\varepsilon_b - \varepsilon_f) \quad (2)$$

A plot of [DNA]/(ε_a – ε_f) vs. [DNA] gave a slope of 1/(ε_b – ε_f) and a Y intercept equal to 1/K_b(ε_b – ε_f); K_b is the ratio of the slope to the Y intercept. Luminescence titration experiments were performed at a fixed metal complex concentration (7 μM) to which increments of a stock DNA solution (0–300 μM) containing the same concentration of the metal complex were added. After the addition of DNA to the metal complex, the resulting solution was allowed to equilibrate at 25 °C in the dark for 10 min before being excited by 450 ± 5 nm light. The data obtained were fitted to Equation (3), where C_T is the concentration of the complex added, C_F is the concentration of the free complex, and I_o and I are the fluorescence intensities in the absence and in the presence of DNA, respectively; P is the ratio of the observed fluorescence quantum yield of the bound complex to the free complex.

$$C_F = C_T[(I/I_o) - P]/[1 - P] \quad (3)$$

The value of P was obtained from a plot of I/I_o vs. 1/[DNA] such that the limiting fluorescence yield is given by the Y intercept. The amount of bound complex (C_B) at any concentration is equal to $C_T - C_F$. A plot of r/C_F vs. r, where $r = C_B$/[DNA], was constructed according to the modified Scatchard equation given by McGhee and Von Hippel [Equation (4)],[57] where K_b is the intrinsic binding constant and n is the binding-site size in base pairs.

$$r/C_F = K_b(1 - nr)\{(1 - nr)/[1 - (n - 1)r]\}^{n-1} \quad (4)$$

DNA melting experiments were carried out by monitoring the absorption (260 nm) of CT DNA (160 μM, nucleotide pairs, NP) with a Shimadzu model UV-160A spectrophotometer coupled with a

temperature controller model Julabo-F12, at various temperatures, in the absence and presence of the complex. The melting temperature (T_m) and the curve width σ_T (temperature range where 10–90% of the absorption increase occurred) were calculated as described previously.[47,58] Viscometric titrations were performed at 25 ± 1 °C with a Cannon-Ubblehode viscometer. Titrations were performed for $[Ru(phen)_3]^{2+}$, $[Ru(phen)_2(aip)]^{2+}$, $[Ru(phen)_2(pyip)]^{2+}$, and ethidium bromide (EtBr; 3–40 μM). Each compound was introduced into the degassed DNA solution (300 μM) present in the viscometer using a Hamilton syringe fitted with a glass extender. Bubbling with nitrogen produced mixing of the drug and DNA. Flow times were measured, with a digital stopwatch, at least three times and were accepted if they agreed within 0.1 s. Reduced specific viscosities were calculated according to Cohen and Eisenberg.[59] Plots of $(\eta/\eta_o)^{1/3}$ (η and η_o are the reduced specific viscosities of DNA in the presence and absence of the drug, respectively) vs. [drug]/[DNA] were constructed. Plots of $(\eta/\eta_o)^{1/3}$ vs. [EtBr]/[DNA] and $[Ru(phen)_3]^{2+}$]/[DNA] were found to be similar to those reported in the literature.[46] For the gel electrophoresis experiments, supercoiled pBR 322 DNA (100 μM in nucleotides) in Tris-HCl buffer (pH = 8.0) was treated with the metal complex (10 μM) and the mixture was incubated in the dark for 1 h. The samples were analyzed by 0.8% agarose gel electrophoresis (Tris-acetate/EDTA buffer, pH = 8.0), stained with EtBr (1 μg/mL, 0.5 h) and then the data were documented with a UVITEC Gel Documentation system. Irradiation experiments were carried out by keeping the pre-incubated (dark, 1 h) samples inside the sample chamber of a JASCO model FP-777 spectrofluorimeter for 60 min (λ_{ex} = 450 ± 5 nm; slit width = 5 nm). The percentage of cleavage (C) was calculated according to Equation (5).

$$C = \frac{[\text{Form II}] + 2[\text{Form III}]}{[\text{Form I}] + [\text{Form II}] + 2[\text{Form III}]} \quad (5)$$

In order to identify the actual reactive oxygen species responsible for DNA damage, a number of control experiments were carried out using various types of quenchers ("inhibitor studies"). Nitrogen gas was used to flush out dioxygen, DABCO (10 mM) was used as a $^1O_2$ quencher, and DMSO (200 mM) and mannitol (100 mM) were used as ·OH scavengers. Tiron (10 mM) was used as a superoxide anion radical quencher.

Acknowledgments

Financial support received for this work from DST New Delhi is gratefully acknowledged. M. M. thanks CSIR for a research fellowship. The authors are thankful to the University Grant Commission, New Delhi, for the facilities provided under the Universities with Potential for Excellence (UPE) programme. We thank Prof. Samudranil Pal for his valuable suggestions.

[1] F. Scandola, C. Chiorboli, M. T. Indelli, M. A. Rampi, *Covalently Linked Systems Containing Metal Complexes*, in *Electron Transfer in Chemistry* (Ed.: V. Balzani), Wiley-VCH, Weinheim, **2001**.
[2] S. O. Kelly, J. K. Barton, in *Metal ions in Biological Systems* (Eds.: A. Sigel, H. Sigel), Marcel Dekker, New York, **1999**, vol. 39, p. 211.
[3] K. E. Erkkila, D. T. Odom, J. K. Barton, *Chem. Rev.* **1999**, *99*, 2777–2795.
[4] A. Kirsch de Mesmaeker, J.-P. Lecomte, J.-M. Kelly, *Top. Curr. Chem.* **1996**, *177*, 25.
[5] A. M. Pyle, J. K. Barton, in *Progress in Inorganic Chemistry* (Ed.: S. J. Lippard), Wiley-Interscience, New York, **1990**, vol. 38, pp. 413–474.
[6] D. S. Sigman, A. Mazumder, D. M. Perrin, *Chem. Rev.* **1993**, *93*, 2295–2316.
[7] S. Satyanarayana, J. C. Dabrowiak, J. B. Chaires, *Biochemistry* **1993**, *32*, 2573–2584.
[8] B. P. Hudson, C. M. Dupureur, J. K. Barton, *J. Am. Chem. Soc.* **1995**, *117*, 9379–9380.
[9] a) P. Lincoln, A. Broo, B. Norden, *J. Am. Chem. Soc.* **1996**, *118*, 2644–2653; b) E. Tuite, P. Lincoln, B. Norden, *J. Am. Chem. Soc.* **1997**, *119*, 239–240.
[10] C. M. Dupureur, J. K. Barton, *J. Am. Chem. Soc.* **1994**, *116*, 10 286–10 287.
[11] C. M. Dupureur, J. K. Barton, *Inorg. Chem.* **1997**, *36*, 33–43.
[12] N. A. P. Kane-Maguire, J. F. Wheeler, *Coord. Chem. Rev.* **2001**, *211*, 145–162.
[13] B. Norden, P. Lincoln, B. Akerman, E. Tuite, in *Metal Ions in Biological Systems* (Eds.: A. Sigel, H. Sigel), Marcel Dekker, New York, **1996**, vol. 33, pp. 177–252.
[14] C. Kaes, A. Katz, M. W. Hosseini, *Chem. Rev.* **2000**, *100*, 3553–3590.
[15] A. E. Friedman, J.-C. Chambron, J.-P. Sauvage, N. J. Turro, J. K. Barton, *J. Am. Chem. Soc.* **1990**, *112*, 4960–4962.
[16] Y. Jenkins, A. E. Friedman, N. J. Turro, J. K. Barton, *Biochemistry* **1992**, *31*, 10 809–10 816.
[17] R. M. Hartshorn, J. K. Barton, *J. Am. Chem. Soc.* **1992**, *114*, 5919–5925.
[18] S. Arounaguiri, B. G. Maiya, *Inorg. Chem.* **1999**, *38*, 842–843.
[19] A. Ambroise, B. G. Maiya, *Inorg. Chem.* **2000**, *39*, 4256–4263.
[20] A. Ambroise, B. G. Maiya, *Inorg. Chem.* **2000**, *39*, 4264–4272.
[21] C. V. Sastri, D. Eswaramoorthy, L. Giribabu, B. G. Maiya, *J. Inorg. Biochem.* **2003**, *94*, 138–145.
[22] B. M. Goldstein, J. K. Barton, H. M. Berman, *Inorg. Chem.* **1986**, *25*, 842–847.
[23] A. M. Pyle, J. P. Rehmann, R. Meshoyrer, C. V. Kumar, N. J. Turro, J. K. Barton, *J. Am. Chem. Soc.* **1989**, *111*, 3051–3058.
[24] Y. Xiong, L.-N. Ji, *Coord. Chem. Rev.* **1999**, *185–186*, 711–733.
[25] L.-N. Ji, X.-H. Zou, J.-G. Liu, *Coord. Chem. Rev.* **2001**, *216–217*, 513–536.
[26] Q.-Z. Zhen, B.-H. Ye, Q.-L. Zhang, J.-G. Liu, H. Li, L.-N. Ji, L. Wang, *J. Inorg. Biochem.* **1999**, *76*, 47–53.
[27] J.-Z. Wu, L. Li, T.-X. Zeng, L.-N. Ji, J.-Y. Zhou, T. Luo, R.-H. Li, *Polyhedron* **1997**, *16*, 103–107.
[28] J.-Z. Wu, B.-H. Ye, L. Wang, L.-N. Ji, J.-Y. Zhou, R.-H. Li, Z.-Y. Zhou, *J. Chem. Soc., Dalton Trans.* **1997**, 1395–1401.
[29] J.-G. Liu, Q.-L. Zhang, X.-F. Shi, L.-N. Ji, *Inorg. Chem.* **2001**, *40*, 5045–5050.
[30] H. Xu, K.-C. Zheng, Y. Chen, Y.-Z. Li, L.-J. Lin, H. Li, P.-X. Zhang, L.-N. Ji, *Dalton Trans.* **2003**, 2260–2268.
[31] V. Xu, K.-C. Zheng, H. Deng, L.-J. Lin, Q.-L. Zhang, L.-N. Ji, *New J. Chem.* **2003**, *27*, 1255–1263.
[32] E. A. Steck, A. R Day, *J. Am. Chem. Soc.* **1943**, *65*, 452–456.
[33] P. Didier, L. Jacquet, A. Kirsch de Mesmaeker, R. Hueber, A. V. Dorsselaer, *Inorg. Chem.* **1992**, *31*, 4803–4809.
[34] a) R. Wang, J. G. Vos, R. H. Schmehl, R. Hage, *J. Am. Chem. Soc.* **1992**, *114*, 1964–1970; b) L.-F. Tan, H. Chao, H. Li, Y.-J. Liu, B. Sun, W. Wei, L.-N. Ji, *J. Inorg. Biochem.* **2005**, *99*, 513–520.
[35] C. V. Kumar, E. H. A. Punzalan, W. B. Tan, *Tetrahedron* **2000**, *56*, 7027–7040.
[36] D. S. Tyson, J. Bialecki, F. N. Castellano, *Chem. Commun.* **2000**, 2355–2356.
[37] J. A. Mondal, G. Ramakrishna, A. K. Singh, H. N. Ghosh, M. Mariappan, B. G. Maiya, T. Mukherjee, D. K. Palit, *J. Phys. Chem. A* **2004**, *108*, 7843–7852.
[38] A. Juris, V. Balzani, F. Barigelletti, S. Campagna, P. Belser, A. V. Zelewsky, *Coord. Chem. Rev.* **1988**, *84*, 85–277.
[39] R. S. Nicholson, I. Shain, *Anal. Chem.* **1964**, *36*, 706–723.

[40] D. P. Rillema, G. Allen, T. J. Meyer, D. C. Conrad, *Inorg. Chem.* **1983**, *22*, 1617–1622.
[41] B. K. Ghosh, A. Chakra-Vorty, *Coord. Chem. Rev.* **1989**, *95*, 239–294.
[42] S. Delaney, M. Pascaly, P. K. Bhattacharya, K. Han, J. K. Barton, *Inorg. Chem.* **2002**, *41*, 1966–1974.
[43] D. J. Patel, *Acc. Chem. Res.* **1979**, *12*, 118–125.
[44] A. L. Lehninger, *Biochemistry*, 2nd ed., Worth Publishers, New York, **1975**, pp. 873–875.
[45] C. V. Kumar, E. H. Asuncion, *J. Am. Chem. Soc.* **1993**, *115*, 8547–8553.
[46] S. Satyanarayana, J. C. Dabrowiak, J. B. Chaires, *Biochemistry* **1992**, *31*, 9319–9324.
[47] J. M. Kelly, A. B. Tossi, D. J. McConnell, C. OhUigin, *Nucl. Acid. Res.* **1985**, *13*, 6017–6034.
[48] B. Armitage, *Chem. Rev.* **1998**, *98*, 1171–1200.
[49] D. D. Perrin, W. L. F. Armarego, D. R. Perrin, *Purification of Laboratory Chemicals*, Pergamon, Oxford, **1986**.
[50] M. Yamada, Y. Tanaka, Y. Yoshimoo, S. Kuroda, I. Shimao, *Bull. Chem. Soc. Jpn.* **1992**, *65*, 1006–1011.
[51] B. P. Sullivan, D. J. Salmon, T. J. Meyer, *Inorg. Chem.* **1978**, *17*, 3334–3341.
[52] E. Austin, M. Gouterman, *Bioinorg. Chem.* **1978**, *9*, 281–298.
[53] I. B. Berlman, in *Handbook of Fluorescence Spectra of Aromatic Molecules*, Academic Press, New York, **1971**.
[54] J. R. Lackowicz, *Principles of Fluorescence Spectroscopy*, Plenum, New York, **1983**.
[55] M. E. Reichmann, S. A. Rice, C. A. Thomas, P. Doty, *J. Am. Chem. Soc.* **1954**, *76*, 3047–3053.
[56] A. Wolfe, G. H. Shimer, T. Meehan, *Biochemistry* **1987**, *26*, 6392–6396.
[57] J. D. McGhee, P. H. Von Hippel, *J. Mol. Biol.* **1974**, *86*, 469–489.
[58] J. Marmur, P. Doty, *J. Mol. Biol.* **1962**, *5*, 109–118.
[59] G. Cohen, H. Eisenberg, *Biopolymers* **1969**, *8*, 45–55.

Received: November 13, 2004

